APPLICATION OF CROSS-BOREHOLE RADAR TO MONITOR FIELD-SCALE VEGETABLE OIL INJECTION EXPERIMENTS FOR BIOSTIMULATION

John W. Lane, Jr., U.S. Geological Survey, Office of Ground Water, Branch of Geophysics, Storrs, CT

Frederick D. Day-Lewis, U.S. Geological Survey, Office of Ground Water, Branch of Geophysics, Storrs, CT; on leave from the Dept. of Geology, Bucknell University, Lewisburg, PA

Roelof J. Versteeg, Idaho National Environmental and Engineering Laboratory, Idaho Falls, ID

Clifton C. Casey, Southern Division Naval Facilities Engineering Command (NAVFAC), North Charleston, SC

Peter K. Joesten, U.S. Geological Survey, Office of Ground Water, Branch of Geophysics, Storrs, CT

Abstract

Cross-borehole radar methods were used to monitor a field-scale biostimulation pilot project at the Anoka County Riverfront Park (ACP), located downgradient of the Naval Industrial Reserve Ordnance Plant, in Fridley, Minnesota. The goal of the pilot project is to evaluate biostimulation using emulsified vegetable oil to treat ground water contaminated with chlorinated hydrocarbons. Vegetable oil is intended to serve as substrate to naturally occurring microbes, which ultimately break down chlorinated hydrocarbons into chloride, carbon dioxide, and water through oxidation-reduction reactions. In support of this effort, cross-borehole radar data were acquired by the U.S Geological Survey in five site visits over 1.5 years. This paper presents level-run (zero-offset profile) and time-lapse radar tomography data collected in multiple planes. Comparison of pre- and post-injection data sets provides valuable insights into the spatial and temporal distribution of both emulsified vegetable oil and also the extent of ground water with altered chemistry resulting from injections—information important for understanding microbial degradation of chlorinated hydrocarbons at the site.

In order to facilitate data interpretation and test the effectiveness of radar for monitoring oil-emulsion placement and movement, three injection mixtures with different radar signatures were used: (1) vegetable oil emulsion, (2) vegetable oil emulsion with a colloidal iron tracer, and (3) vegetable oil emulsion with a magnetite tracer. Based on petrophysical modeling, mixture (1) is expected to increase radar velocity and decrease radar attenuation relative to background—a water-saturated porous medium; mixtures (2) and (3) are expected to increase radar velocity and also increase radar attenuation due to their greater electrical conductivity compared to native ground water.

Radar slowness (inverse radar velocity) tomograms and level-run profiles show decreases in slowness in the vicinity of injection wells. Slowness anomalies are observed only in planes connected to injection wells, indicating that the emplaced emulsified vegetable oil does not migrate far after injection. In contrast to the localization of slowness anomalies, attenuation anomalies are observed in all level-run profiles, particularly those downgradient of the injection wells. Despite the expected signatures of different tracers, increases in attenuation are observed downgradient of all three injections; thus, we infer that the attenuation changes do not result from the iron tracers. One viable explanation for the observed attenuation changes is that products of oil-enhanced biodegradation (for example, ferrous iron) increase electrical conductivity of ground water and thus radar attenuation.

Application of radar methods to data from the ACP demonstrated the utility of radar for monitoring biostimulation. Results of level-run and tomographic surveys identified (1) the distribution of emulsified vegetable oil, and (2) the distribution of ground water with oil-affected chemistry. Ongoing research efforts include simultaneous tomographic inversion of radar data from multiple planes, petrophysical modeling, geostatistical interpolation, and development of an integrated interpretation considering conventional borehole logs and surface-to-borehole radar data.

Introduction

In biostimulation, a material (for example, emulsified vegetable oil) is introduced into the subsurface to enhance bioremediation by serving as substrate to native microbes, which ultimately transform chlorinated hydrocarbons into carbon dioxide, water, and chloride by oxidation-reduction reactions. Biostimulation relies on proper emplacement of the substrate in contact with the contaminant and in sufficient concentration to support microbial activity. Lane and others (2003) evaluated the use of cross-borehole radar methods to monitor injections of vegetable oil emulsion and support the design and operation of biostimulation efforts. Petrophysical modeling, synthetic examples, and analysis of field experimental data indicated that radar methods can provide valuable information about the spatial distribution of emulsified vegetable oil. Inversion of tomographic radar travel-time data from one image plane clearly indicated the location of injected vegetable oil emulsion. The pore-fluid replacement of water by emulsified oil manifested as a well-defined radar-slowness anomaly. In this study, we present additional field experimental data acquired between multiple boreholes in the vicinity of the Naval Industrial Reserve Ordnance Plant (NIROP), in Fridley, Minnesota.

The U.S. Geological Survey (USGS) acquired five sets of cross-borehole radar data over the course of 1.5 years to monitor the emplacement and movement of the vegetable oil emulsion and resulting changes in ground-water chemistry at the Anoka County Riverfront Park (ACP), located downgradient of the NIROP (figs. 1, 2). The purpose of the U.S. Naval Facilities Engineering Command (NAVFAC), Southern Division pilot project is to assess biostimulation using emulsified vegetable oil for remediation of chlorinated hydrocarbons including trichloroethene (TCE) and dichloroethene (DCE), which are present in ground water at the site (CH2M Hill Constructors, Inc., 2002).

Methods

Cross-Borehole Radar

Two radar survey geometries are considered in this study: (1) cross-hole level-run or zero-offset profiling, and (2) cross-hole tomography. In the level-run geometry, measurements are collected with the transmitter antenna located at multiple depths in one borehole, and the receiver antenna located at identical depths in a second borehole (fig. 3a). In tomography, the transmitter antenna is located at multiple depths in one borehole, and for each transmitter location, the receiver antenna is located at multiple depths in a second borehole (fig. 3b). High-frequency electromagnetic (EM) waves propagate from the transmitter, and waveform traces are recorded at receiver locations. Whereas tomographic data can be analyzed to estimate cross-sectional images (tomograms) of radar slowness or attenuation, level-run data provide only horizontally averaged layer slowness or attenuation measurements. Although level-run data are less informative about spatially variable radar properties and thus the distribution of vegetable oil emulsion, acquisition of level-run data is much faster, and measurements that level-runs comprise tend to have higher signal-to-noise owing to shorter raypaths and stronger antenna radiation in the horizontal direction.

Measurements of radar-wave travel-time and amplitude are used to estimate radar slowness (the inverse of radar velocity) or attenuation, respectively. If data are collected at multiple times, then it is possible to calculate and invert difference data to generate tomograms (in the case of tomography data) or profiles (in the case of level-run data) of difference slowness or difference attenuation. Increasingly, hydrogeologists and engineers are looking to such time-lapse information to facilitate interpretation of tracer migration (Niva and others, 1988; Hubbard and others, 2001; Singha and others, 2003; Day-Lewis and others, 2003), unsaturated-zone dynamics (Eppstein and Dougherty, 1998; Binley and others, 2001), leakage through engineered barriers (Ramirez and others, 1996; Binley and others, 1997), and natural hydrologic processes, such as tide-driven salinity changes (Slater and Sandberg, 2000). Lane and others (2003) first demonstrated the effectiveness of radar for monitoring vegetable oil biostimulation.

The use of radar methods for time-lapse monitoring of injection experiments relies on the contrasts between the dielectric permittivity and/or electrical conductivity of the injectate relative to those of native ground water. The slowness of radar-wave propagation is a strong function of dielectric permittivity, which is determined by pore fluid, porosity, saturation, and the soil or rock matrix. The attenuation of radar waves is a strong function of electrical conductivity, which is determined by total dissolved solids, the chemical composition of the pore fluid, and the soil or rock matrix. Because the relative dielectric permittivity of vegetable oil is much lower than that of water (ε_r^{oil} ~2.9-3.5; $\varepsilon_r^{H_2O}$ ~80), the presence of emulsified vegetable oil in the saturated zone is expected to decrease radar slowness (increase radar velocity). Due to the greater electrical resistivity of oil relative to that of native ground water at ACP, the presence of emulsified oil in the saturated zone is expected to decrease radar attenuation; however, the addition of magnetite and colloidal-iron tracers to emulsified vegetable oil makes the electrical conductivity of the resulting mixtures much greater than that of native ground water. Also, the electrical conductivity of ground water in contact with or downgradient of the vegetable oil emulsion may be elevated compared to native ground water because of microbial activity that results in reduced mineral species, such as the reduction of ferric to ferrous iron in ground water.

Tomographic Inversion Methods

Tomographic inversion typically involves an optimization problem to identify the two-dimensional (2-D) or three-dimensional (3-D) slowness or attenuation model that minimizes a weighted combination of (1) errors between predicted and measured data in a least-squares sense, and (2) a measure of solution complexity, for example, roughness or deviations from a mean value. Numerous algorithms have been employed for this purpose, including the simultaneous iterative reconstruction technique (SIRT) (for example, Dines and Lytle, 1979; McMechan and others, 1987; Hyndman and others, 1994), LSQR (for example, Bregman and others, 1989), and conjugate-gradients (for example, Olsson and others, 1992). Most approaches involve parameterizations that discretize the interwell region as a grid of 2-D pixels or 3-D voxels; however, the geophysical literature includes some innovative parameterizations based on objects or shapes (Lane and others, 2003), data-driven zones (Eppstein and Dougherty, 1998), natural pixels (Michelena and Harris, 1991), staggered and adapted grids (Vesnaver and Böhm, 1999, 2000), wavepaths (Vasco and others, 1995), and fresnel volumes (Červený and Soares, 1992). In this study, a weighted damped least-squares algorithm (Lane and others, 2003) was used to invert each tomography data set; the resulting image is then refined to better match the level-run data set using a SIRT algorithm. This step places greater weight on level-run data, which in our experience are more reliable than measurements for higher-angle raypaths included in the tomography data. Borehole deviations are accounted for by projecting data to a best-fit image plane between transmitter and receiver boreholes. The tomographic inversion is implemented in Matlab[1].

---

[1] The use of firm, trade, and brand names in this report is for identification purposes only and does not constitute endorsement by the U.S. Government.

Field Experiment

The radar data presented here were collected from nine PVC boreholes at a well field in the ACP (fig. 1). The boreholes are cased with 3-in. inner-diameter PVC and completed to depths of between 12.2 and 22.6 m. The site is underlain by glacial drift and glacial-fluvial deposits consisting of unconsolidated coarse- to fine-grained sand and silts (CH2M Hill Constructors, Inc., 2002). Oil emulsion injections were performed in boreholes INJ-1, INJ-2, and INJ-3 on December 11-12, 2001. Three injection mixtures with different radar signatures were evaluated: (1) 4,542 liters of 65 percent native water and 35 percent soybean oil and a lecithin emulsifier were injected in INJ-2; (2) 4,542 liters of 65 percent native water and 35 percent soybean oil and a lecithin emulsifier and 3.5 kg of dissolved magnetite were injected in INJ-3; and (3) 4,542 liters of 65 percent native water and 35 percent soybean oil and a lecithin emulsifier and 50 kg of colloidal iron were injected in INJ-1. Based on petrophysical modeling and lab experiments (Lane and others, 2003), mixture (1) was expected to increase radar velocity and decrease radar attenuation relative to background—a water-saturated porous medium; (2) and (3) were expected to increase radar velocity and also increase radar attenuation due to their greater electrical conductivity relative to native ground water. The magnetite tracer remained in solution, but the colloidal iron settled out quickly during the injection. Boreholes INJ-1, INJ-2, and INJ-3 were screened over depth intervals of 10.67 to 13.72 m below ground surface (bgs). At the time of the injections, the water table in the vicinity of the boreholes was about 8 m bgs; thus, the tops of the well screens were about 2.5 m below the water table.

Radar data were acquired with a Malå GeoScience RAMAC borehole-radar system using broad-band electric-dipole antennas with a center frequency in air of about 100 MHz. Five rounds of data collection were conducted between December 2001 and June 2003, including pre- and post-injection surveys. In total, level-run data were collected at one or more times between 17 borehole pairs; and tomography data were collected at least once for 15 image planes. Tomography data collection focused on planes MW-07 to INJ-3 and MW-01 to INJ-2. Surface-to-borehole radar data and conventional borehole geophysical logs, including natural gamma, electromagnetic induction, neutron, borehole deviation, and magnetic susceptibility were also collected; however, analysis and presentation of these data are outside the scope of this paper. Rather, we focus here on the level-run and tomography data, from which we construct a conceptual model of the spatial and temporal distributions of (1) emulsified vegetable oil and (2) the extent of ground water with altered chemistry resulting from the injections and possibly enhanced microbial activity. Development of an integrated conceptual model of the spatial and temporal distribution of emulsified vegetable oil and biostimulation-affected ground water is the topic of ongoing research.

Level-run data were collected in 0.2-m depth increments, with the transmitter antenna in one borehole, and the receiver antenna in a second borehole at the same depth from top of casing. For tomography surveys, the transmitter antenna was positioned at different locations in one borehole, and the receiver antenna was moved from the top to the bottom of a second borehole, with measurements triggered at 0.2-m depth increments. A representative transmitter-receiver geometry used for tomography surveys is shown in figure 4 for the plane between boreholes INJ-3 and MW-07. The tomography data set includes measurements for 325 raypaths, each measurement corresponding to a unique transmitter-receiver combination.

Results and Discussion

The primary goal of the geophysical surveys collected at the ACP site is to characterize the spatial and temporal distributions of both vegetable oil emulsion and the region of the subsurface where

ground-water chemistry has been affected by oil-enhanced microbial activity or chemistry changes accompanying injection, such as the reduction of ferric to ferrous iron. This objective is achieved through inspection of level-run data and tomograms for individual planes, and cross-comparison of level-run data and tomograms for different planes. Planes for which radar travel-times or amplitudes show significant changes from background data sets are interpreted as being inside the oil-affected region, whereas planes for which all data sets are similar are interpreted as being outside the affected region.

Level-Run Results and Interpretation

Level-run slowness profiles (estimated as radar-wave travel-time divided by borehole offset distance) are shown for planes MW-07 to INJ-3, MW-06 to MW-01, INJ-3 to INJ-2, MW-07 to MW-02 in Figures 5a to 8a, respectively. In this discussion, we focus primarily on the saturated zone below the depth of 10 m, where the effect of the vegetable oil emulsion is observed. Above the water table, changes in radar slowness may result from natural water-table fluctuation and temporal variations in saturation.

Significant changes in slowness in the saturated zone are observed only in planes connected to injection wells. In planes including two injection boreholes (for example, the INJ-2 to INJ-3 plane, fig. 7a) or an injection borehole and a borehole upgradient of the injection (for example, the BG-01 to INJ-2 plane, not shown), slowness anomalies are observed to persist in time but diminish somewhat in magnitude, presumably due to slow movement of emulsified oil out of these planes in the direction of ground-water flow. Conversely, some planes involving boreholes downgradient of injection wells show increases in slowness anomaly magnitude over time (for example, the MW-07 to INJ-3 plane, fig. 5a), presumably resulting from movement of emulsified oil into these planes. Level-run slowness data from November of 2002 show no significant changes along the transect defined by boreholes MW-06, MW-01, and MW-07 (fig. 6a) or in plane MW-02 to MW-07 (fig. 8a) downgradient of the injections. Based on the spatial and temporal distribution of slowness anomalies, we infer that the vegetable oil emulsion had not spread horizontally more than 4 or 5 m from the injection boreholes by November of 2002. A qualitative, highly idealized map of the interpreted extent of subsurface emulsified vegetable oil in November 2002 is shown in figure 9.

There is some evidence of vertical movement of oil emulsion in the level-run slowness data. In several profiles, for example in the MW-07 to INJ-3 and INJ-3 to INJ-2 planes (figs. 5a and 7a, respectively), negative peaks in the slowness curve appear to migrate downward in the interval from 18- to 20-m depth, even though the vegetable oil emulsion has a lower density than water. Directly above the water table, increases in slowness relative to air could indicate a "pancake" of lighter-than-water, pure-phase vegetable oil; however, this is difficult to determine without additional, supporting information.

In contrast to the localization of slowness anomalies, attenuation anomalies are not confined to planes including injection boreholes. Significant changes in attenuation are observed in all level-run planes, though the anomalies are not present at all times. Level-run peak-to-peak (P-P) amplitude profiles are shown in figures 5b to 8b for the MW-07 to INJ-3, MW-06 to MW-01, INJ-3 to INJ-2, MW-07 to MW-02 planes, respectively. In some planes, attenuation anomalies increase in magnitude for a period of time, peak, then diminish; in other planes, anomalies increase only during the 1.5-year period of data collection. Figures 6b and 8b show changes in radar attenuation in the planes between boreholes MW-06 and MW-01, and between MW-07 and MW-02, respectively, but no significant change in radar slowness. This indicates changes in ground-water chemistry in the absence of emulsified vegetable oil. By November 2002, attenuation changes were observed in the MW-06 to MW-01 and MW-07 to MW-01 planes. Although no level-run data were collected in November 2002 in the MW-01 to MW-02 plane, data from June 2003 also show no changes in slowness but appreciable changes in attenuation. Based on

these results, a qualitative map of the interpreted extent of oil-affected ground water in November 2002 is inferred (fig. 9).

Depth intervals where changes in attenuation are greater or occur earlier in the study period are interpreted as indicative of more permeable and/or porous sedimentary layers, where oil-affected ground water penetrates more deeply or in greater quantity. For example, between 15- and 17-m depth in the MW-07 to INJ-3 level-run data (fig. 5b), the observed radar-wave amplitudes show large decreases, indicating increased attenuation and, thus, elevated electrical conductivity. This attenuation anomaly is found at similar depths in the four level-run profiles presented (fig. 5b-8b), indicating that the layer transmitting oil-affected ground water at these depths is present in the MW-07 to INJ-3, MW-06 to MW-01, INJ-3 to INJ-2, and MW-07 to MW-02 cross sections.

Tomography Results and Interpretation

Data collection for tomography focused on the two planes from MW-07 to INJ-3 and MW-01 to INJ-2. In previous work (Lane and others, 2003), we presented results for the MW-07 to INJ-3 plane and evaluated the effects of regularization and limited resolution on application of petrophysical models to estimate oil-emulsion saturation. We concluded for this data set that interpretation of anomaly magnitude and extent is complicated by blurring and other artifacts owing to limited data, limited angular coverage, data errors, and regularization. Despite these limitations, radar slowness tomograms provide valuable information about the distribution of emulsified vegetable oil, and radar attenuation tomograms provide valuable information about the distribution of ground water with altered chemistry resulting from injections of emulsified vegetable oil.

A powerful method for exploratory analysis of cross-borehole radar data and identification of anomaly extent is to compare plots of (1) raypaths for measurements showing large changes in slowness or attenuation and (2) raypaths for measurements showing small or insignificant changes in slowness or attenuation. For data collected in December 2001, figure 10a shows raypaths in the MW-7 to INJ-3 plane with difference-slowness values above the median value for the data set, that is, measurements that do not indicate decreases in radar slowness or the presence of vegetable oil emulsion. Figure 10b shows raypaths in the same plane for which difference-slowness values are below the 30th percentile of the data set, that is, measurements that indicate significant decreases in slowness, and possibly the presence of vegetable oil emulsion. Comparison of figures 10a and 10b enables visualization of the interwell region where emulsified vegetable oil is likely found. This region extends from INJ-3 toward MW-07, but appears to pinch out toward MW-07.

Difference-slowness tomograms for December 2001 for the MW-07 to INJ-3 and MW-01 to INJ-2 planes are shown in Figure 11a and 11b, respectively. The presence of emulsified vegetable oil appears as blue, negative-slowness difference anomalies in both planes. The location and extent of the anomaly in the MW-07 to INJ-3 plane are qualitatively consistent with the raypath plots of figure 10. In both tomograms, the anomalies extend away from the injection well toward the monitoring wells. The actual region affected by oil is likely smaller than the estimated anomalies, as blurring and streaking of anomalies are expected due to the underdetermined nature of most tomographic inverse problems.

Conclusions

Cross-borehole radar monitoring of biostimulation using emulsified vegetable oil was shown to provide valuable insights into the spatial and temporal distribution of both the vegetable oil emulsion and the extent of ground water with altered chemistry. Specifically, travel-time data proved useful for identifying the distribution of vegetable oil emulsion, which remained close to the three injection wells. Amplitude data were useful for identifying changes in ground-water chemistry, presumably due to the

impact of the injected vegetable oil emulsion on ground-water chemistry; over time, radar attenuation, and thus electrical conductivity, increased downgradient of the injection wells. The change does not appear to result from the colloidal-iron or magnetite tracers alone, as the attenuation change is observed downgradient from all three injections. Biologically induced transformation of the aquifer sediments could also explain the field data. The injections of emulsified vegetable oil could promote reduction of ferric iron to mobile ferrous iron, which could also increase electrical conductivity.

In ongoing work, we seek to extend the results presented here. Research efforts include (1) correlation of cross-borehole radar results with conventional borehole geophysical logs, surface-to-borehole radar, and water chemistry data to develop an integrated interpretation of the injection experiments; (2) simultaneous, multiple-plane inversion of tomographic and level-run data sets to provide a more reliable 3D interpretation of changes in the subsurface resulting from the injection experiments; and (3) application of petrophysical models (Lane and others, 2003) to the combined, 3D results to provide estimates of spatially variable saturation of vegetable oil emulsion.

References

Binley, A., P. Winship, R. Middleton, M. Pokar, and J. West, 2001, High resolution characterization of unsaturated zone dynamics using cross-borehole radar: Water Resources Research, v. 37, no. 11, p. 2639-2652.

Binley, A., W. Daily and A. Ramirez, 1997, Detecting leaks from environmental barriers using electrical current imaging: J. Environmental and Engineering Geophysics, v. 2, no. 1, 11-19.

Bregman, N.D., R.C. Bailey, and C.H. Chapman, 1989, Crosshole seismic tomography: Geophysics, v. 54, no. 2, p. 200-215.

Červený, V., and J.E.P. Soares, 1992, Fresnel volume ray tracing: Geophysics, v. 57, no. 7, p. 902-915.

CH2M Hill Constructors, Inc., 2002, Pilot-scale study to enhance in-situ bioremediation of chlorinated solvents via vegetable oil injection at Anoka County Riverfront Park, Naval Industrial Reserve Ordnance Plant Fridley, Fridley, Minnesota: Atlanta, Georgia, CH2M Hill Constructors, Inc., CD ROM.

Day-Lewis, F. D., J. W. Lane, Jr., J. M. Harris, and S. M. Gorelick, 2003, Time-lapse imaging of saline tracer tests using cross-borehole radar tomography: Water Resources Research, v. 39, no. 10, 1290, doi:10.1029/2002WR001722.

Dines, K. A., and R. J. Lytle, 1979, Computerized geophysical tomography: Proc. IEEE, v. 67, p. 1065-1073.

Eppstein, M.J. and D. E. Dougherty, 1998, Efficient three-dimensional data inversion; soil characterization and moisture monitoring from cross-well ground-penetrating radar at a Vermont test site: Water Resources Research, v. 34, no. 8, 1889-1900.

Frederickson, J.K., F.J. Brockman, G.P. Streile, J.W. Cary, and J.F. McBride, 1993, Enhancement of in-situ microbial remediation of aquifers: US Patent number US 5,265,674/A/, Patent and trademark office, Box 9, Washington, DC 20232.

Hubbard, S., J. Chen, J. Peterson, E. Majer, K. Williams, D. Swift, B. Mailliox, and Y. Rubin, 2001, Hydrogeological characterization of the D.O.E. bacterial transport site in Oyster Virginia using geophysical data: Water Resources Research, v. 37, no. 10, p. 2431-2456.
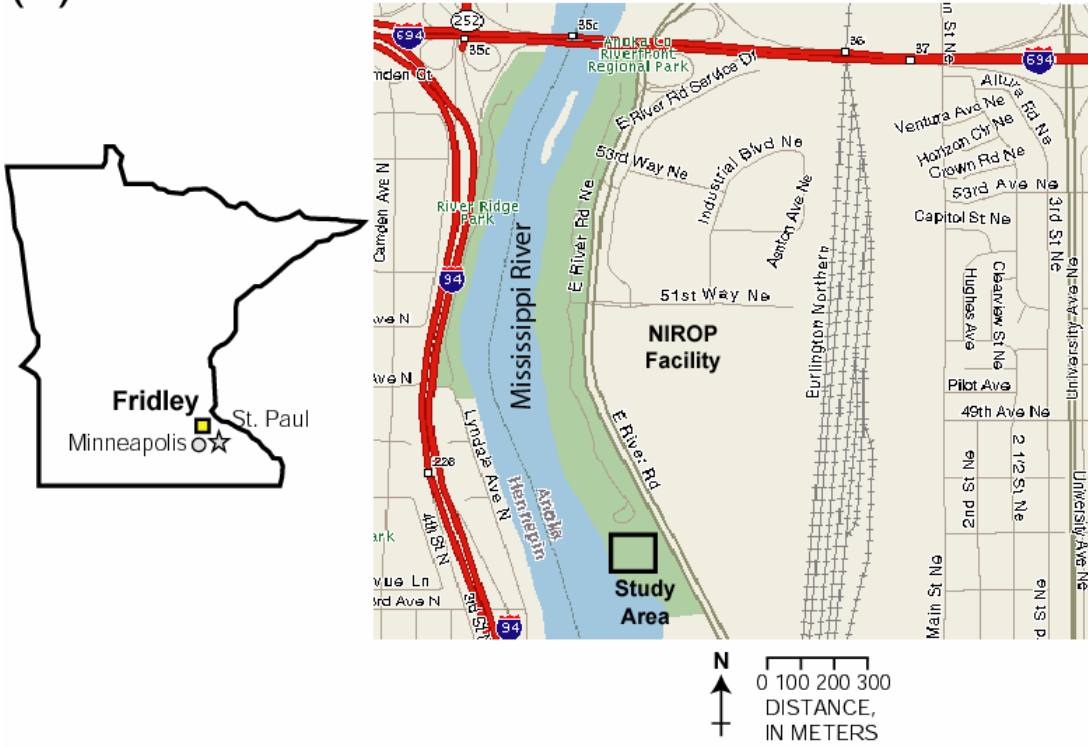
Hutter, J.C., G.F. Vandegrift, L. Nunez, and D.H. Redfield, 1994, Removal of VOCs from groundwater using membrane-assisted solvent extraction: AICHE Journal, v. 40, no. 1, p. 166-177.

Hyndman, D. W., J. M. Harris, and S. M. Gorelick, 1994, Coupled seismic and tracer test inversion for aquifer property characterization: Water Resour. Res., vol. 30, no. 7, 1965-1977.

Lane, J.W., Jr., F.D. Day-Lewis, J.M. Harris, F.P. Haeni, and S.M. Gorelick, 2000, Attenuation-difference radar tomography--results of a multiple-plane experiment at the U.S. Geological Survey Fractured Rock Research Site, Mirror Lake, New Hampshire, *in* Noon, D.A., Stickley, G.F., and Longstaff, D., eds., International Conference on Ground Penetrating Radar, 8th, Proceedings: University of Queensland, Queensland, Australia, p. 666-675.

Lane, J.W., Jr., Day-Lewis, F.D., Versteeg, R.J., and Casey, C.C., 2003, Object-based inversion of crosswell radar tomography data to monitor vegetable oil injection experiment, *in* Symposium on the Application of Geophysics to Engineering and Environmental Problems (SAGEEP), April 6-10, 2003, San Antonio, Texas, Proceedings: Denver, Colorado, Environmental and Engineering Geophysical Society, CD-ROM, 27 p.

McMechan, G.A., J.M. Harris, and L.M. Anderson, 1987, Cross-hole tomography for strongly variable media with applications to scale model data: Bull. Seismol. Soc. Am., v. 77, no. 6, p. 1945-1960.

Michelena, R. and J. M. Harris, 1991, Tomographic traveltime inversion using natural pixels: Geophysics, v. 5, no. 5, 635-644.

Niva, B., O. Olsson, and P. Blumping, 1988, Radar cross-hole tomography at the Grimsel Rock Laboratory with application to migration of saline tracer through fracture zones: Nationale Genossenschaft fur die lagerung radioaktiver Abfalle, NTB 88-31.

Olsson, O., L. Falk, O. Forslund, L. Lundmark, and E. Sandberg, 1992, Borehole radar applied to the characterization of hydraulically conductive fracture zones in crystalline rock: Geophysical Prospecting, v. 40, no. 2, p. 109-142.

Ramirez, A., W. Daily, A. M. Binley, A. LaBrecque, D. Roelant, 1996, Detection of leaks in underground storage tanks using electrical resistance methods: J. Environmental and Engineering Geophysics, v. 1, no. 3, 189-203.

Singha, K., A. M. Binley, J. W. Lane, Jr., and S. M. Gorelick, 2003, Electrical Imaging of Tracer Migration at the Massachusetts Military Reservation, Cape Cod, *in* Symposium on the Application of Geophysics to Engineering and Environmental Problems (SAGEEP), April 6-10, 2003, San Antonio, Texas, Proceedings: Denver, Colorado, Environmental and Engineering Geophysical Society, CD-ROM, 10 p.

Slater, L.D., and S. K. Sandberg, 2000, Resistivity and induced polarization monitoring of salt transport under natural hydraulic gradients: Geophysics, v. 65, no. 2, 408-420.

Vasco, D.W., J.E. Peterson, Jr., and E.L. Majer, 1995, Beyond ray tomography--wavepaths and Fresnel volumes: Geophysics, v. 60, p. 1790-1804.

Vesnaver, A., and G. Böhm, 1999, In quest of the grid: Geophysics, v. 64, no. 4, p. 1116-1125.

Vesnaver, A., and G. Böhm, 2000, Staggered or adapted grids for seismic tomography: The Leading Edge, v. 19, p. 944-950.
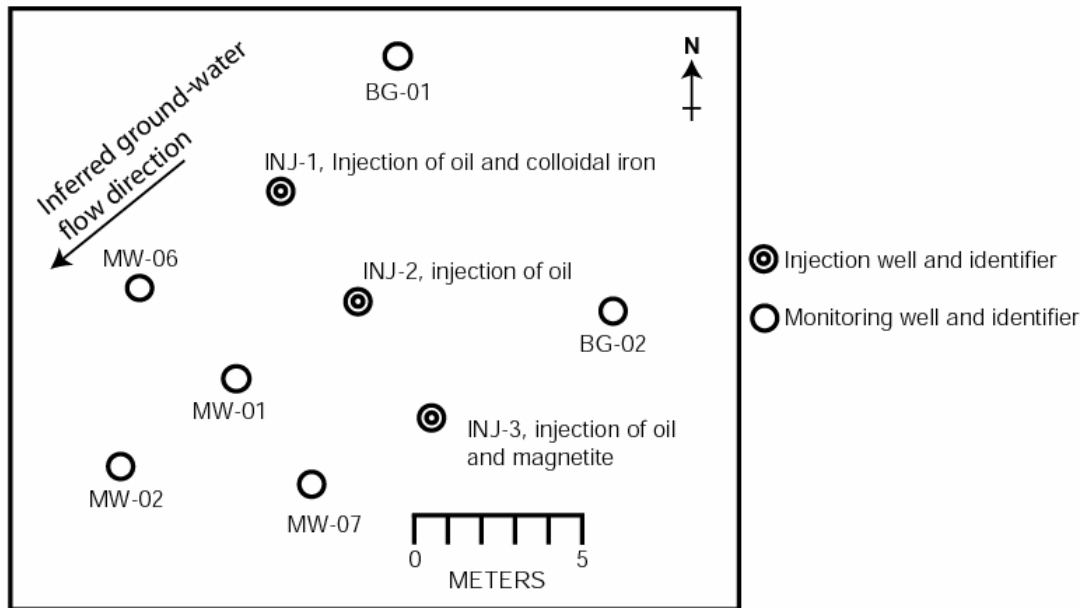
Acknowledgments

Figure 1.: (a) Location of the study area, Anoka County Riverfront Park, near the Naval Industrial Ordnance Plant (NIROP), Fridley, Minnesota. (b) Map of the well field in the study area.

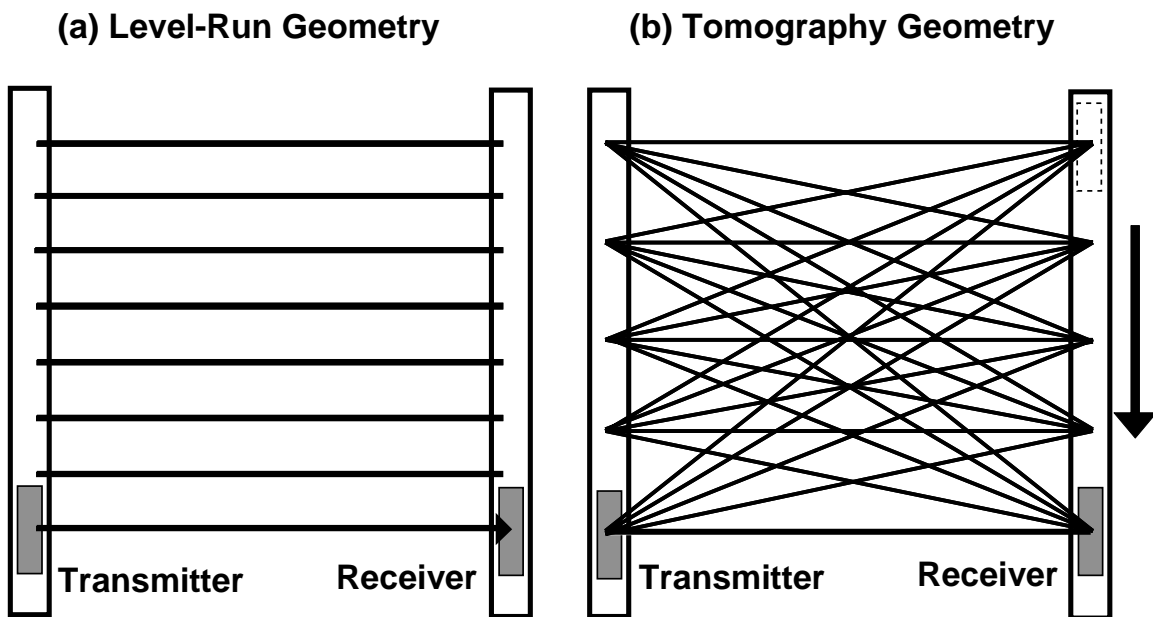**Figure 2.:** Photograph of the field site, looking west (downgradient) toward the Mississippi River.

Figure 3.: (a) Level-run radar raypath geometry, in which measurements are made with transmitter and receiver antennas located at identical depths. (b) Tomography raypath geometry, in which for each transmitter position, measurements are made for multiple receiver positions.
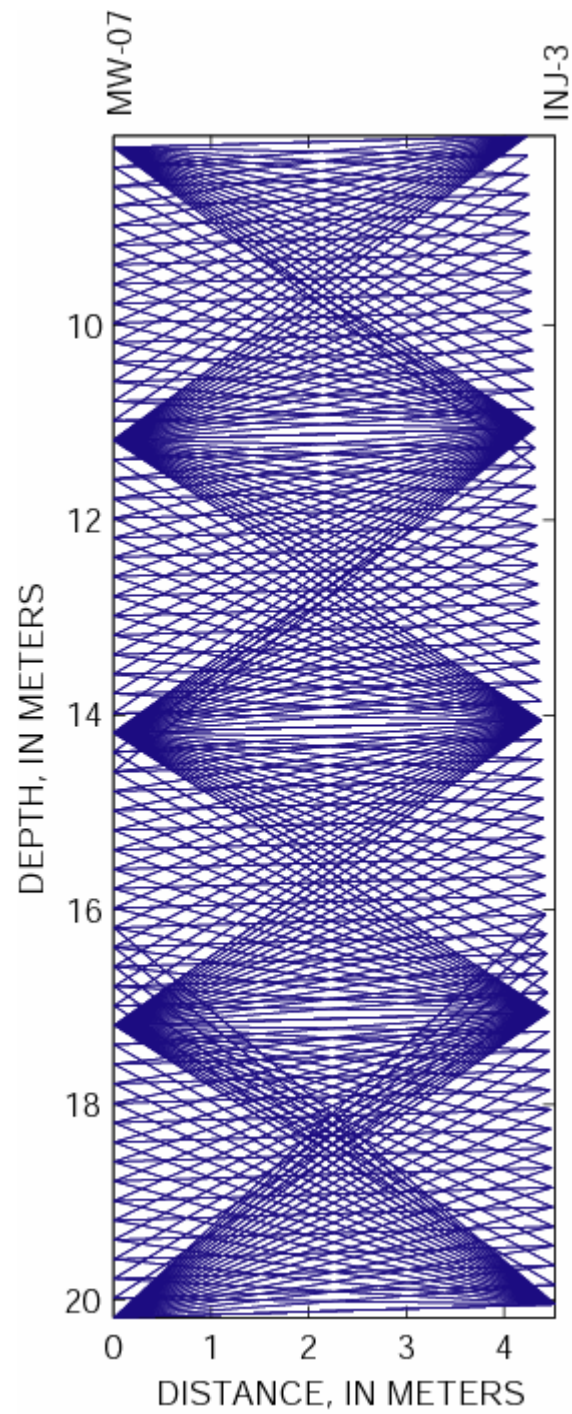
Figure 4.: Cross-borehole transmitter-receiver geometry used for tomography data collection in the MW-07 to INJ-3 plane.
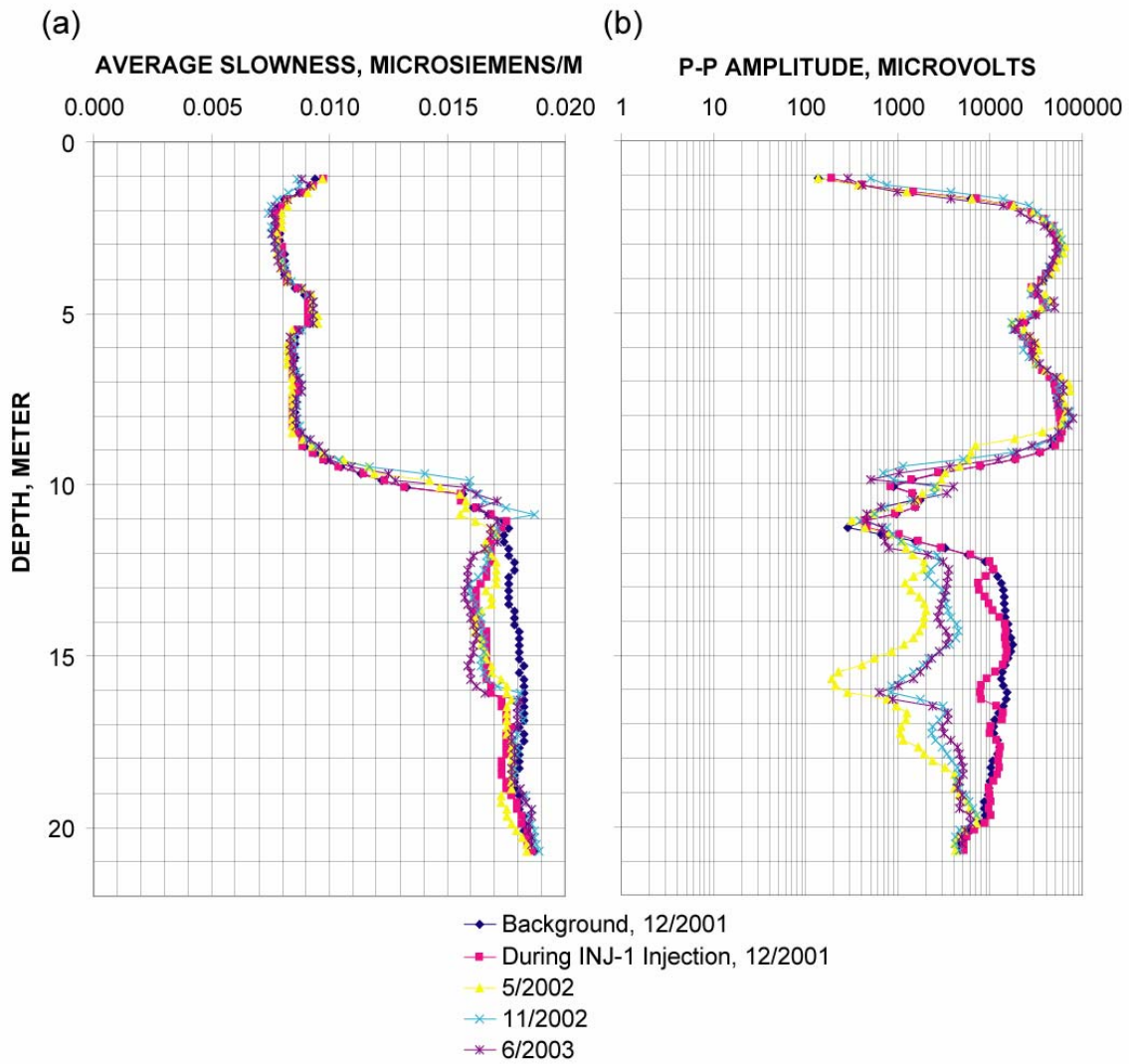
Figure 5.: (a) Level-run slowness profile for the MW-07 to INJ-3 plane. (b) Level-run peak-to-peak (P-P) amplitude profile for the MW-07 to INJ-3 plane.
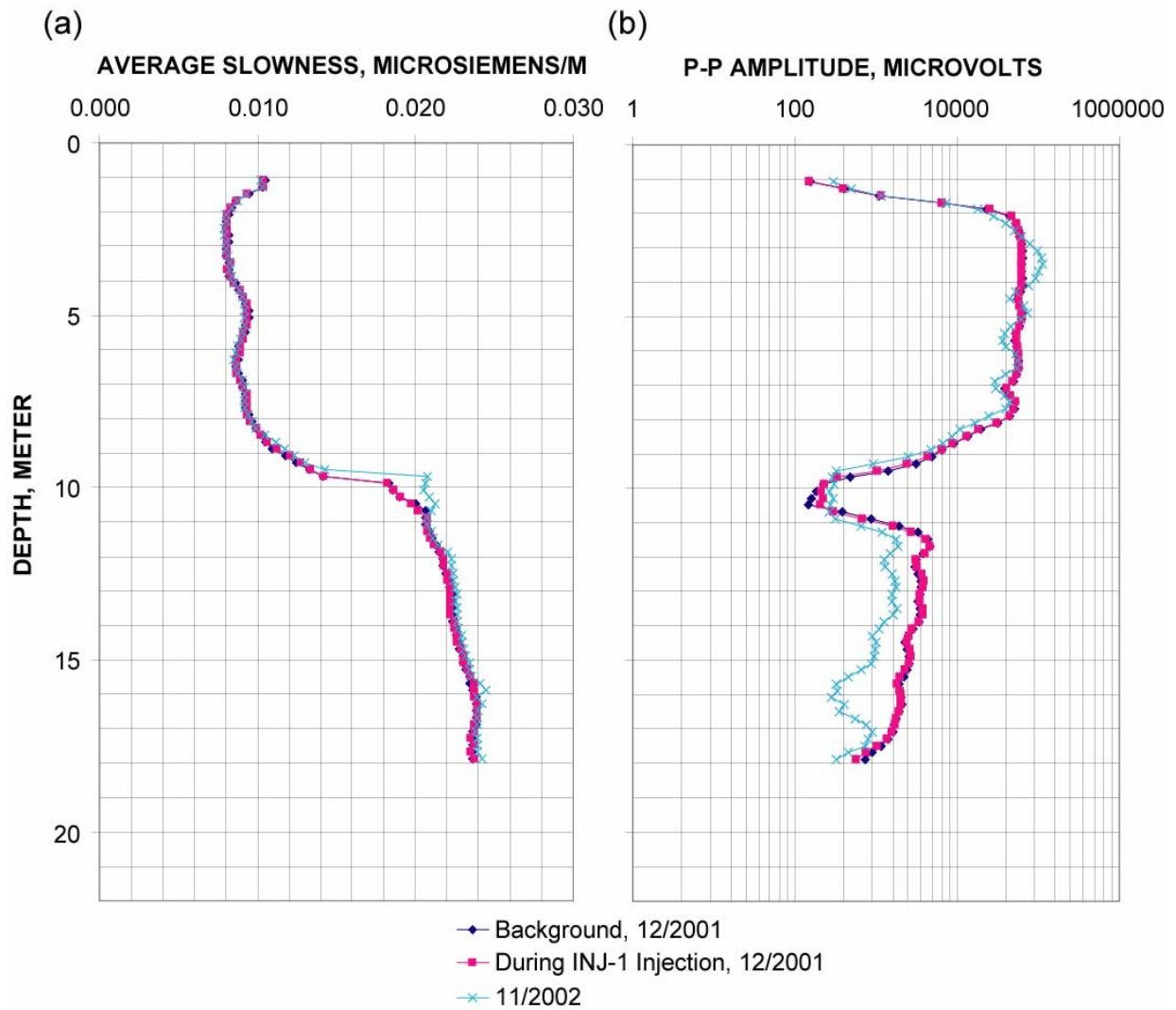
Figure 6.: (a) Level-run slowness profile for the MW-06 to MW-01 plane. (b) Level-run peak-to-peak (P-P) amplitude profile for the MW-06 to MW-01 plane.
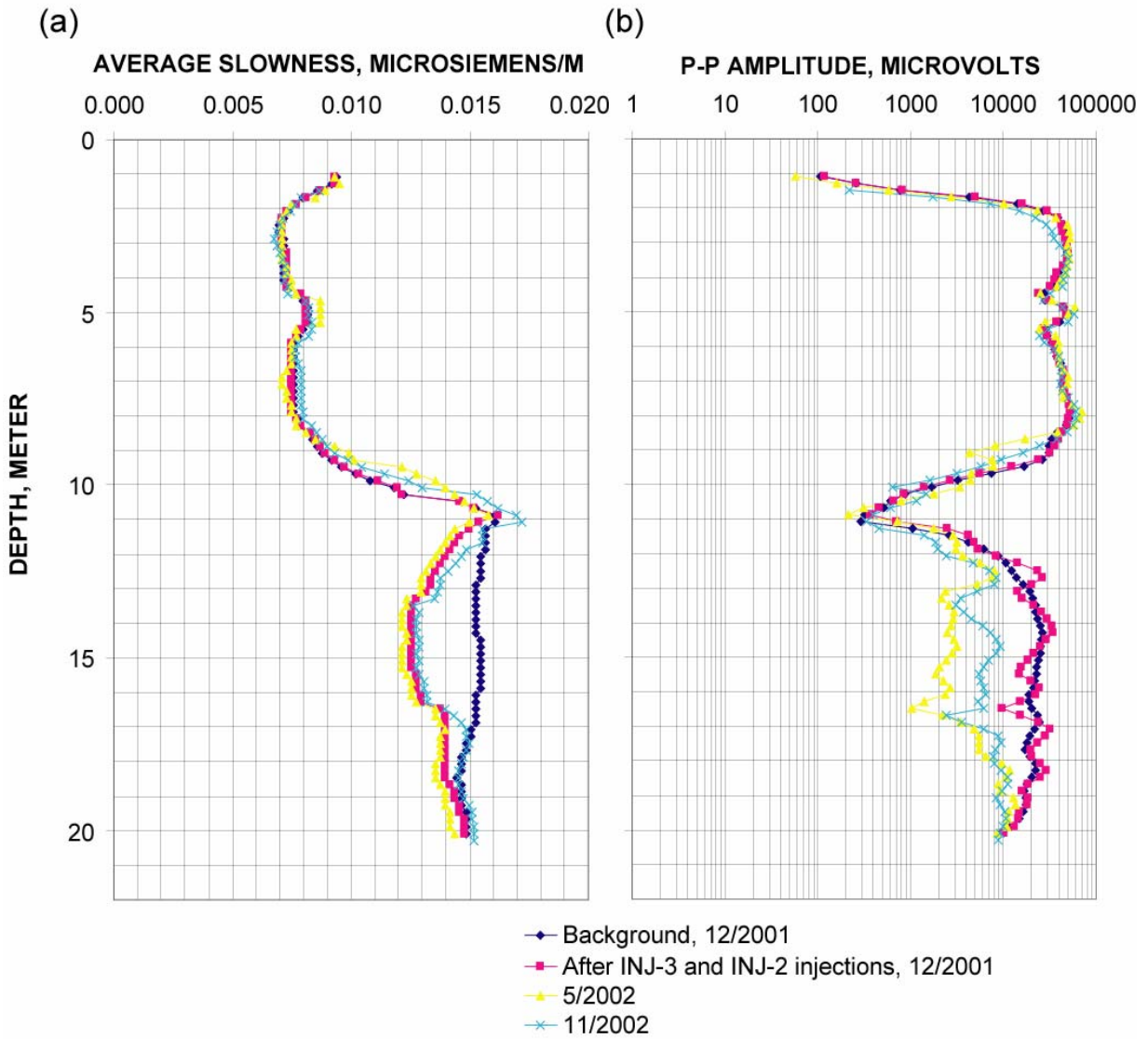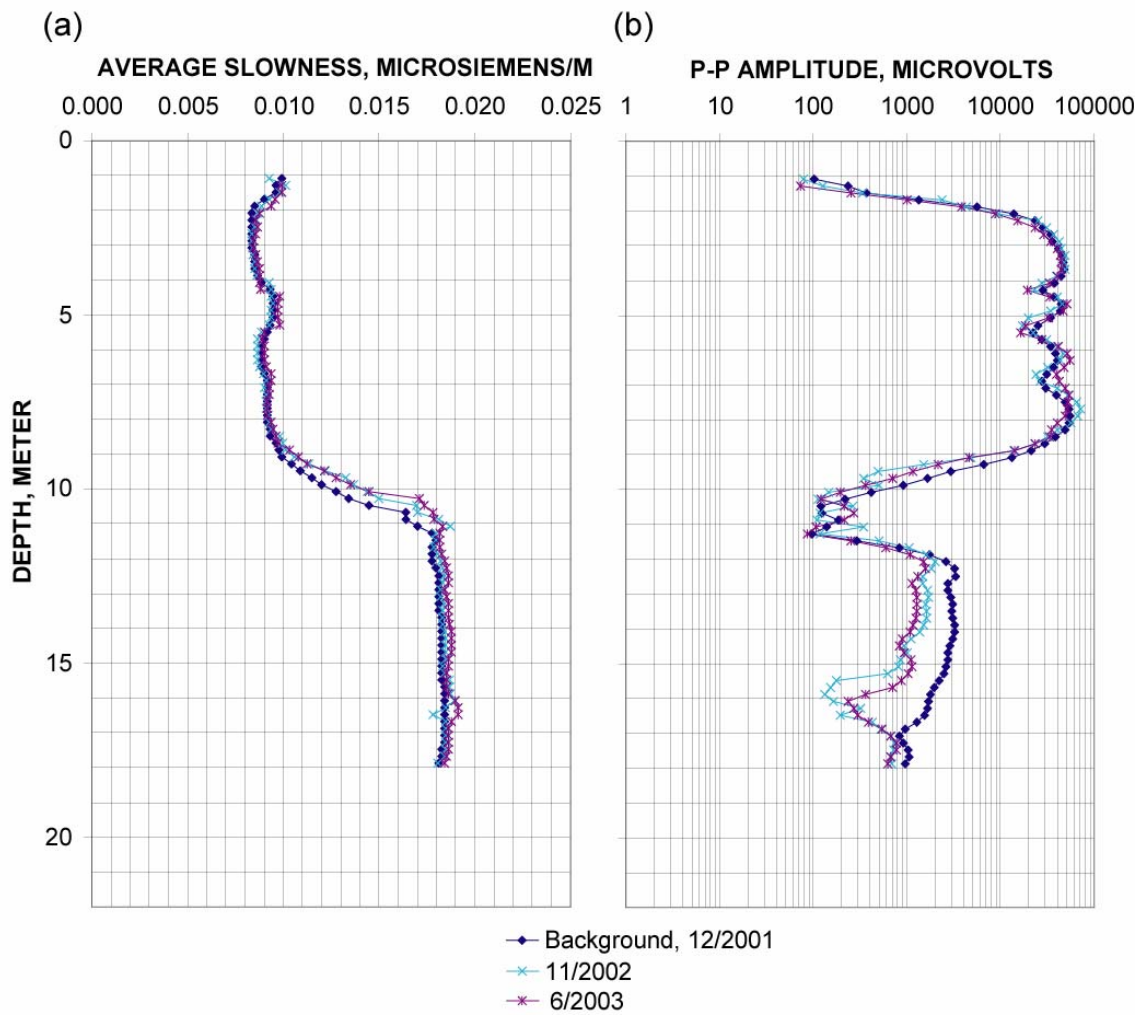
Figure 7.: (a) Level-run slowness profile for the INJ-3 to INJ-2 plane. (b) Level-run peak-to-peak (P-P) amplitude profile for the INJ-3 to INJ-2 plane.

Figure 8.: (a) Level-run slowness profile for the MW-07 to MW-02 plane. (b) Level-run peak-to-peak (P-P) amplitude profile for the MW-07 to MW-02 plane.
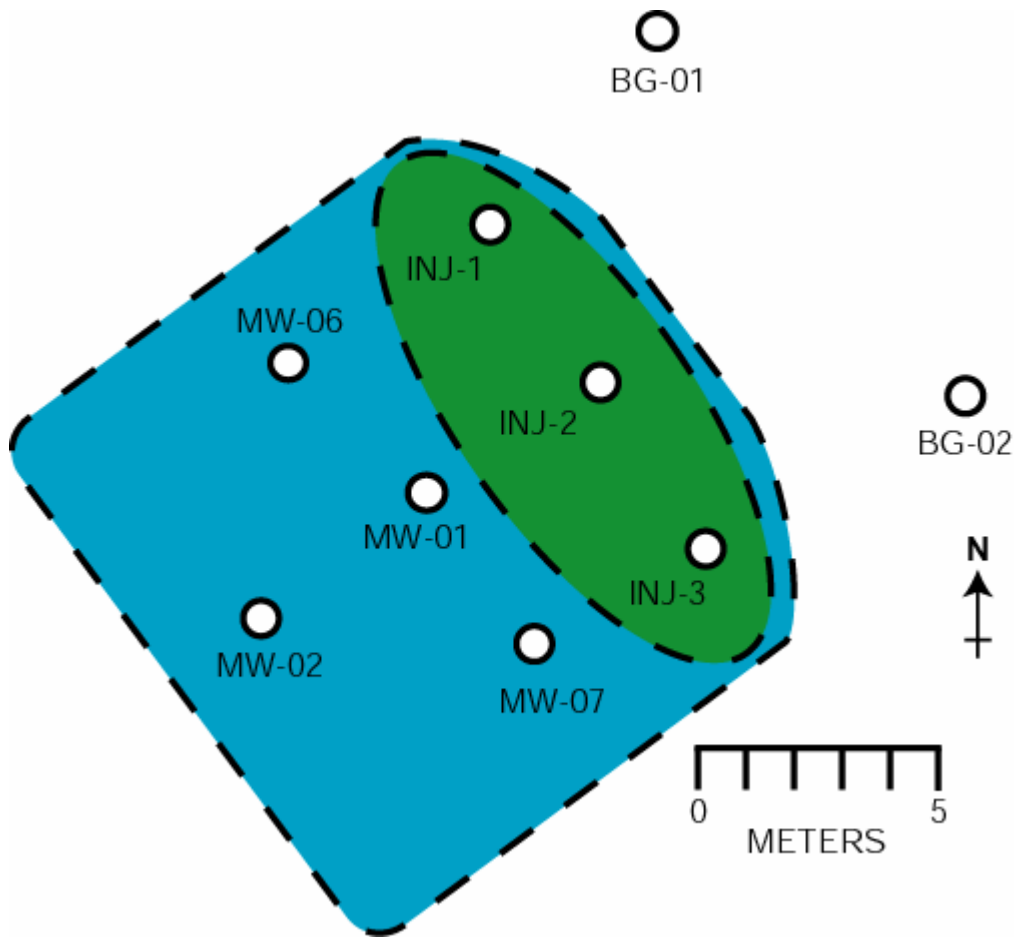
Figure 9.: Qualitative interpretation of the extent of subsurface vegetable oil emulsion (shown in green) and the extent of oil-affected ground water (shown in blue) in November 2002. Boundaries are idealized and approximated.
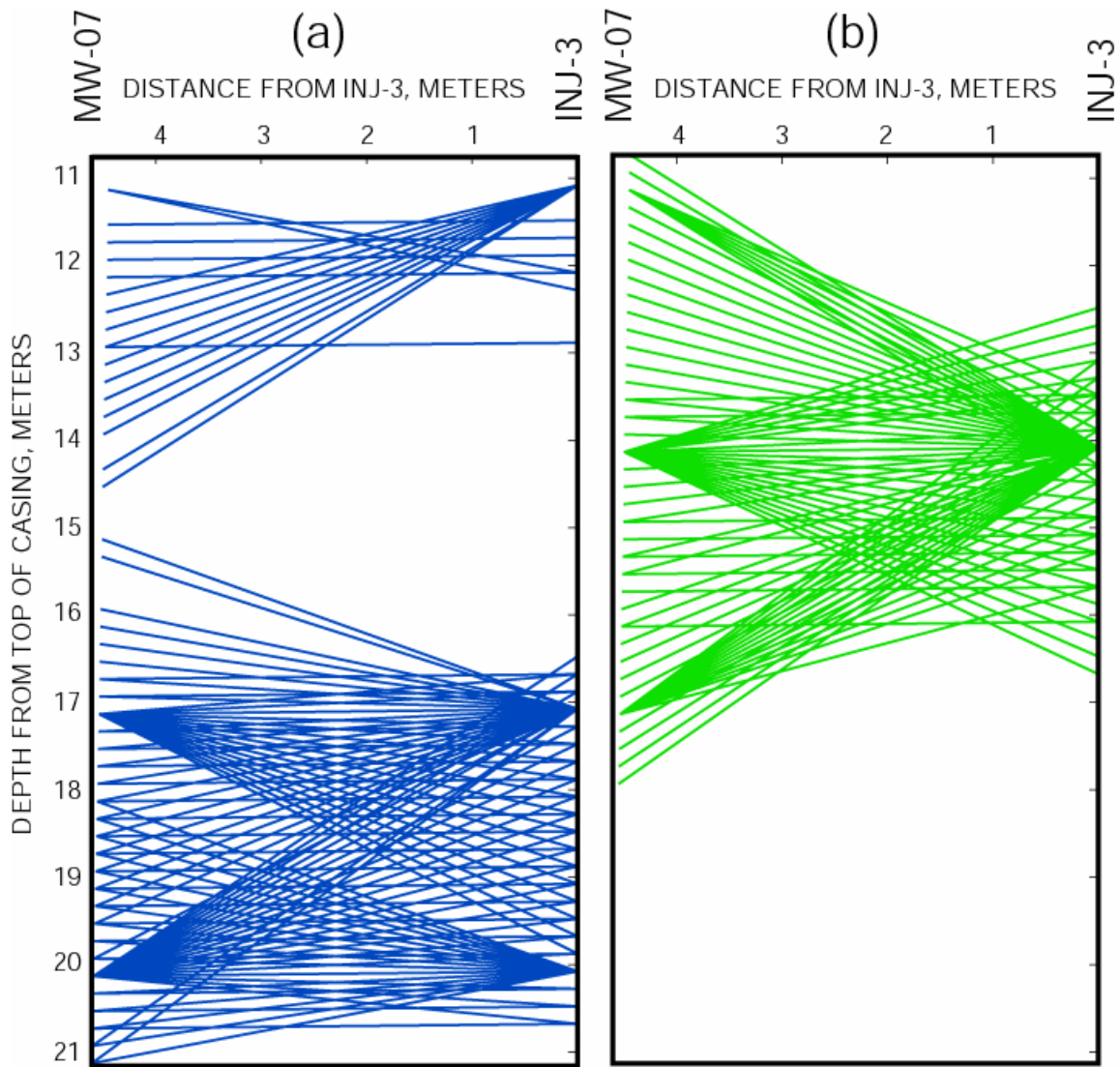
Figure 10.: (a) Raypaths corresponding to difference-slowness data of greater than the median value of the data set. (b) Raypaths corresponding to difference-slowness data showing less than the 30th percentile. Relatively large decreases in attenuation are observed along raypaths shown in green, presumably resulting from replacement of pore water by vegetable oil emulsion. Raypaths shown in blue seem largely unaffected by the oil injection.
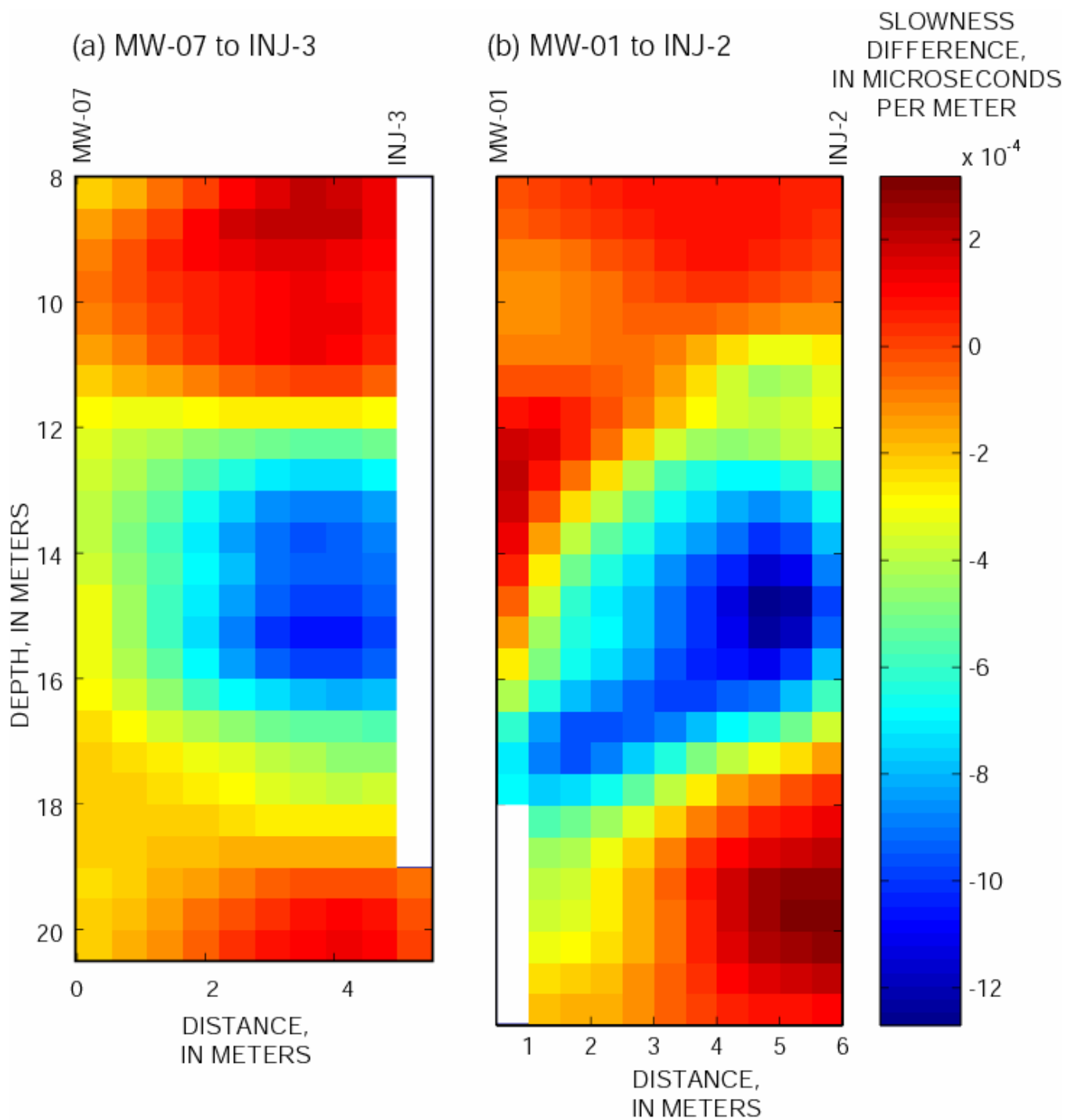
Figure 11. (a) Radar slowness tomogram for the MW-7 to INJ-3 plane in December 2001, and (b) radar slowness tomogram for the MW-1 to INJ-2 plane in December 2001.